nature nanotechnology

ARTICLES

https://doi.org/10.1038/s41565-022-01111-6

Probing nanomotion of single bacteria with graphene drums

Irek E. Rosłoń[1,2], Aleksandre Japaridze[1,2], Peter G. Steeneken[1], Cees Dekker[1] and Farbod Alijani[1]✉

Motion is a key characteristic of every form of life[1]. Even at the microscale, it has been reported that colonies of bacteria can generate nanomotion on mechanical cantilevers[2], but the origin of these nanoscale vibrations has remained unresolved[3,4]. Here, we present a new technique using drums made of ultrathin bilayer graphene, where the nanomotion of single bacteria can be measured in its aqueous growth environment. A single *Escherichia coli* cell is found to generate random oscillations with amplitudes of up to 60 nm, exerting forces of up to 6 nN to its environment. Using mutant strains that differ by single gene deletions that affect motility, we are able to pinpoint the bacterial flagella as the main source of nanomotion. By real-time tracing of changes in nanomotion on administering antibiotics, we demonstrate that graphene drums can perform antibiotic susceptibility testing with single-cell sensitivity. These findings deepen our understanding of processes underlying cellular dynamics, and pave the way towards high-throughput and parallelized rapid screening of the effectiveness of antibiotics in bacterial infections with graphene devices.

Living cells exhibit nanomechanical vibrations as a result of the biological processes that govern their growth, function and reproduction[5]. This nanomotion is an intriguing phenomenon of unravelled origin that has been observed in a wide variety of living organisms, including neuronal cells[6], erythrocytes, yeasts[7,8] and bacteria[4]. Numerous hypotheses have been proposed for the underlying driving mechanism, such as motion of organelles, internal redistribution of cell membranes[9] and the action of ion pumps[3], but consensus has not been reached[4]. This relates to the fact that non-invasive probing of biomechanics at the microscale is highly challenging, which has stimulated the development and application of techniques such as atomic force microscopy[10–12] (AFM), optical and magnetic tweezers[13], flow cytometry[14] and optical tracking of cells[15,16]. In particular, for bacterial cells, micromechanical cantilevers have emerged as powerful tools for detecting vibrations of adhered cell populations (100–1,000 bacteria) in a liquid environment[4]. It was shown that the nanomotion of these populations rapidly decreases in the presence of antibiotics, which holds great promise for the development of rapid antibiotic susceptibility testing technologies[2]. Both for probing fundamental biomechanical processes and for development of nanomotion-based antibiotic susceptibility tests in medical diagnostics, it is crucial to explain the microscopic origins of nanomotion.

Here, we present a new single-cell technique based on suspended graphene drums[17], which greatly enhances the sensitivity of nanomechanical sensing compared to previous cantilever-based methods. The ultra-high sensitivity of the technique allowed us to clarify the mechanism that lies at the root of bacterial nanomotion by probing various strains of *E. coli*. The small mass, high stiffness and micrometre-sized area of a suspended graphene drum enables detecting nanomotion at even the single-bacterium level. Using arrays of these drums, we compare the vibrations produced by different *E. coli* strains. In particular, we investigate the contributions of the bacterial cell-wall synthesis, flagella, rotor and ion pump to nanomotion, and demonstrate that flagellar motion is the main source of nanomotion in these bacteria. Moreover, by tracing the nanomotion in the presence of antibiotics, we show that this new ultrasensitive graphene-based platform enables antibiotic susceptibility tests with single-bacterium sensitivity. This opens new routes towards faster, label-free detection of antimicrobial resistance at the single-cell level with potential applications in drug screening and rapid diagnostics.

Graphene drums for probing a single bacterium. The experiments were performed using drums made of an ultrathin (<1 nm) bilayer of chemical vapour-deposited graphene that covered circular cavities with a diameter of 8 µm and a depth of 285 nm that were etched in SiO_2. A silicon chip with an array of thousands of these graphene-covered cavities was placed inside a cuvette containing *E. coli* in Luria-Bertani (LB) medium, where (3-aminopropyl) triethoxysilane (APTES) was used to bind the bacteria to the graphene surface (Supplementary Note 1 and Methods). The nanomotion of a bacterium resulted in a deflection of the suspended membrane, which was measured using laser interferometry[18] (Fig. 1a). The bacterium induced a time-dependent deflection $z(t)$ at the centre of the suspended graphene drum, which can be determined from the modulation of the intensity of the reflected light[19]. To quantitatively compare the nanomotion of different drums, we acquired $z(t)$ traces over 30-s periods to obtain the variance $\sigma^2 = \langle z^2(t) \rangle$, or the motion amplitude σ, which we used as a measure of the magnitude of the nanomotion.

Drums containing a single live bacterium (Fig. 1b–d) displayed large displacements z_{max} of up to 60 nm, with a time averaged motion amplitude of up to $\sigma = 20$ nm, that clearly exceed the deflection of drums without bacteria and signal from cells deposited on the Si/SiO_2 substrate away from the drums, which yielded a background $\sigma = 2$ nm (Fig. 1e and Supplementary Notes 2 and 3). The large oscillation amplitudes can be associated with the movement of the suspended drum and originate from bacterial biophysical processes. To characterize the motion further, we recorded the signal of a single bacterium for more than 1 hour. It is apparent that fluctuations were present that show similarities over different timescales (Fig. 2a).

[1]Delft University of Technology, Delft, the Netherlands. [2]These authors contributed equally: I. E. Rosłoń, A. Japaridze. ✉e-mail: f.alijani@tudelft.nl

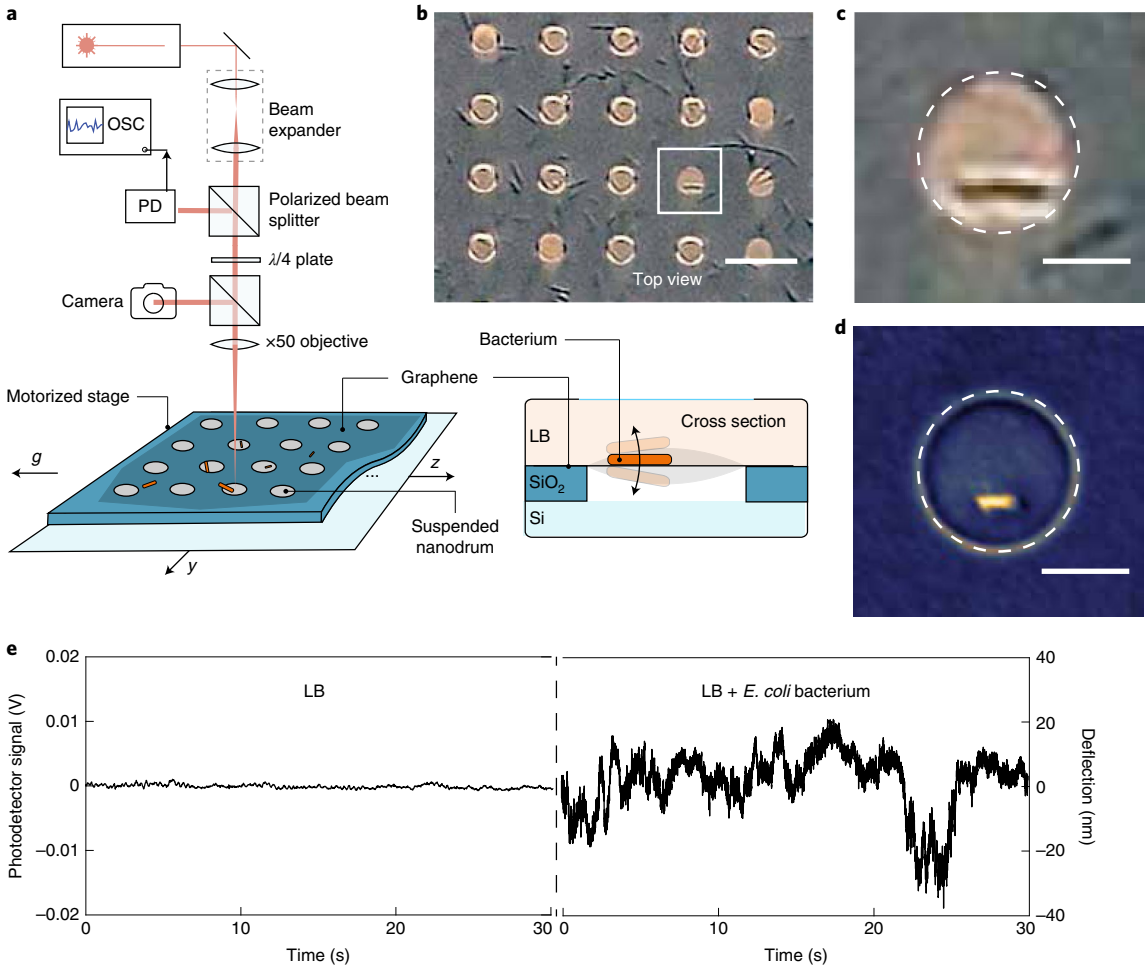

Fig. 1 | Detection of nanomotion of single bacteria by graphene drums. a, Schematic of the interferometric measurement setup used to record the nanomotion. OSC and PD stand for oscilloscope and photodiode, respectively. **b**, Optical microscope image of an array of suspended drums with adhered *E. coli*. Scale bar, 20 µm. **c**, Zoom in of the area indicated by a white square in **b**, showing a dividing bacterium on top of a graphene drum. Scale bar, 5 µm. **d**, Scanning electron microscopy image of an *E. coli* on a suspended graphene drum. Scale bar, 5 µm. **e**, Recorded deflection of a suspended graphene drum immersed in LB without a bacterium (left), compared to the signal from a graphene drum with a bacterium present (right).

Fluctuations were also observed on timescales ranging from seconds to hours. Figure 2b displays the power spectral density (PSD) of the motion (black line), compared to the background signal of an empty drum. The spectra have a $1/f^{\alpha}$ frequency dependence, with a mean value of $\alpha = 1.8 \pm 0.1$ ($n = 277$ graphene drums; Fig. 2c). The difference between drums with and without a single bacterium can also be clearly perceived by listening to audio recordings that were generated by converting the interferometric traces to a sound track (provided as Supplementary Audio). These results are consistent with power spectral densities found for bacterial colonies on AFM cantilevers[20], and show that the nanomotion generated by even a single *E. coli* bacterium lacks a specific periodicity but instead involves a wide range of frequencies.

Impact of flagellar motility on nanomotion. While various origins of nanomotion have been proposed[3,4], we speculate that flagellar motility constitutes the main source. To clarify its role on the bacterial forces generated, we compare the nanomotion of four *E. coli* strains (Fig. 3a) that were genetically modified to have varying levels of motility: a hyper-motile strain with a larger number of flagella compared to wildtype, a minimally motile strain that lacks the regulatory IS1 element for the flagellum synthesis[21,22], a non-motile strain with disabled flagellar motors and a flagella-less strain where the motors are functional but flagella are lacking. As a fifth case, we studied the overall influence of ion pumps on the nanomotion by administering cadaverine, a drug, that blocks ionic transport through the cell membrane[23] and thus reduces cell motility.

The histograms in Fig. 3b compare the motion of hyper-motile bacteria before and after exposure to cadaverine. The motion amplitude σ is observed to be substantially lowered after adding the drug (the median reduced from $\sigma = 13.4$ nm to 7.0 nm before and after administering cadaverine, respectively), indicating that the bacterial motion was strongly reduced, although it did not get fully quenched. The level of motility was observed to have a large influence on the magnitude of the nanomotion signal, as shown in Fig. 3c. We observed that the nanomotion from the strains with both functional flagella and motors (median of $\sigma = 13.4$ nm for hyper-motile and $\sigma = 12.6$ nm for minimally motile strains) was significantly larger than from strains in which either the motor was disabled or the flagella was removed (median variance $\sigma = 5.3$ nm for non-motile and $\sigma = 2.6$ nm for flagella-less strains). We conclude that the observed differences in nanomotion are mainly induced by the activity of flagella, since the nanomotion disappeared in the flagella-less strain and the amplitude clearly correlates with the activity of the flagella.

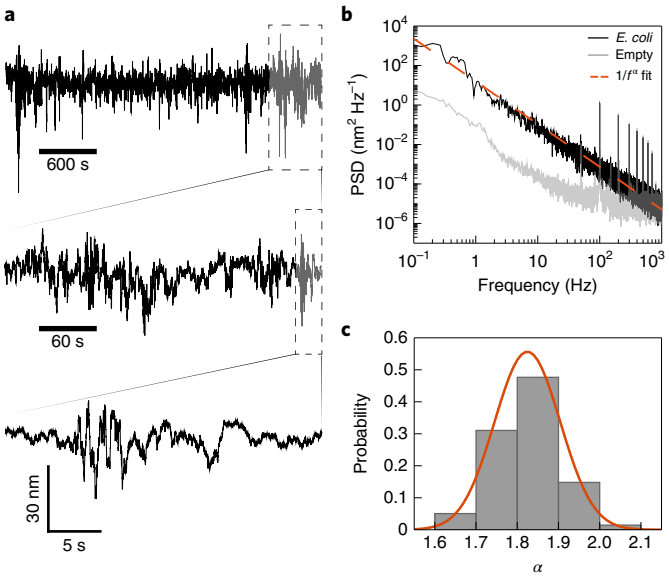

Fig. 2 | Motion of a single bacterium. a, Deflection $z(t)$ versus time for a graphene drum with a single *E. coli* in LB, recorded for 1 h. By zooming in on the part indicated in grey, while maintaining the same y axis scale, it is observed that fluctuations are present over a wide range of timescales. **b**, Amplitude PSD of the time trace shown in **a**, of a live bacterium (black) and for the baseline from an empty drum (grey). Dashed orange line is a fit to $1/f^{\alpha}$ spectrum with $\alpha = 2.1$. The background spectrum is significantly lower and shows enhanced noise at frequencies below 1 Hz and a flatter noise spectrum above 100 Hz. Peaks appear at harmonics of 50 Hz due to mains interference. **c**, Probability distribution of α from fitting $1/f^{\alpha}$ noise. Orange line represents a Gaussian fit to the distribution, yielding an average value of $\alpha = 1.8 \pm 0.1$ (mean ± s.d.) ($n = 277$ samples).

Antibiotic susceptibility tests on single bacteria. Subsequently, we explored whether antibiotic susceptibility tests can be performed on single *E. coli* bacteria by monitoring nanomotion of graphene drums. To test the efficacy of different antibiotics, we measured the nanomotion variance σ^2 of each drum for 30 s, both before and 1 hour after administering an antibiotic above its minimum inhibitory concentration. Figure 4a shows the six different antibiotics that we tested and their mode of action. For the antibiotics rifampicin, ciprofloxacin, 2,4-Dinitrophenol (DNP) and chloramphenicol, a decrease in the nanomotion was observed (Fig. 4b–f and Table 1). Initially, a median motion amplitude $\sigma = 7$ nm is observed for the AB1157 *E. coli* strain, but quickly after administering the antibiotic the amplitudes drop to median values around $\sigma = 3$ nm. The cells are not viable after antibiotic treatment, as the motion does not increase back to its original level when the antibiotic is flushed out with LB (Supplementary Fig. 7, similar to earlier reports[2]). These results show that one can use graphene drums for testing antibiotic susceptibility on the basis of nanomotion.

To test whether graphene drums are able to distinguish resistant cells, we used *E. coli* cells with a chromosomal *KanR* resistance gene[24]. When these cells were exposed to kanamycin, we observed no change in the motion amplitude ($\sigma \cong 5$ nm) (Fig. 4d). However, when we subsequently exposed the same cells to chloramphenicol, we did observe a decrease in the signal with respect to the initial nanomotion (down to $\sigma = 1.8$ nm). Additionally, we treated *E. coli* cells with A22, which alters cell-wall synthesis. We used subminimum inhibitory concentrations of the drug, such that the bacteria lose their typical rod shape and become rounded (Supplementary Note 4) without killing the cells or impairing their division and motility[25–28]. In contrast to the effect of the other antibiotics, the variance of cells grown in presence of A22 was found to be similar to that of the untreated cells, and disruption of the cell-wall synthesis was not observed to result in a reduction in the nanomotion.

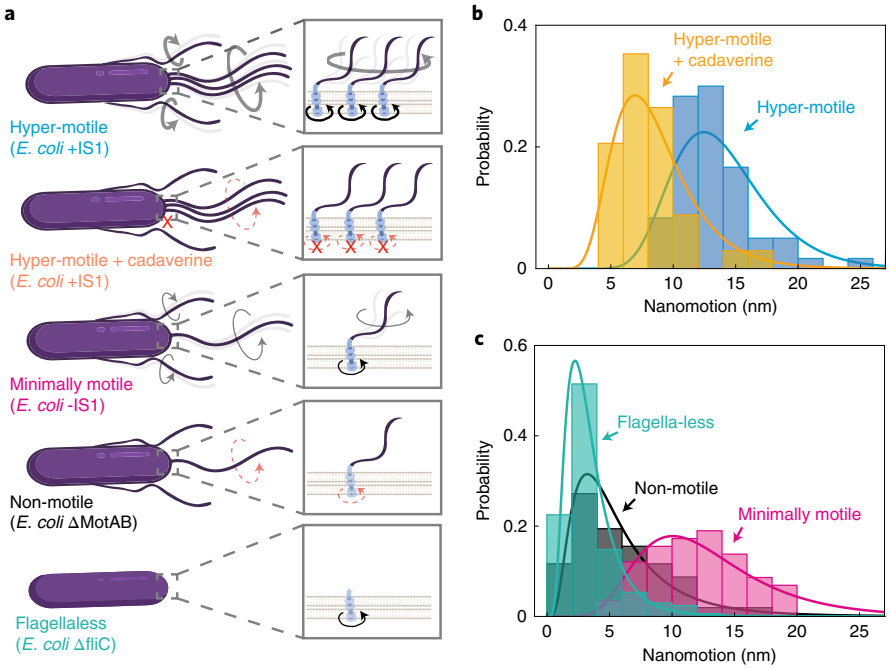

Fig. 3 | Impact of flagellar motility on nanomotion. a, To study the influence of motility on nanomotion, the following strains are compared: hyper-motile, hyper-motile with motility impaired by cadaverine, minimally motile by a genetic blocker, non-motile by gene deletion (MotAB) and flagella-less (fliC). Red cross indicates a blocked ion pump and red dashed arrow indicates a disabled motor. **b**, Histogram of the motion amplitude σ of hyper-motile bacteria before (blue, $n = 60$) and after (yellow, $n = 34$) administering cadaverine, showing reduction of nanomotion. **c**, Motion σ of minimally motile *E. coli* (purple, $n = 58$) is compared to the non-motile strain (black, $n = 103$) and the flagella-less strain (turquoise, $n = 169$). The non-motile and flagella-less strains showed significantly lower motion than the minimally motile strain. Lines represent lognormal fits to the distributions.

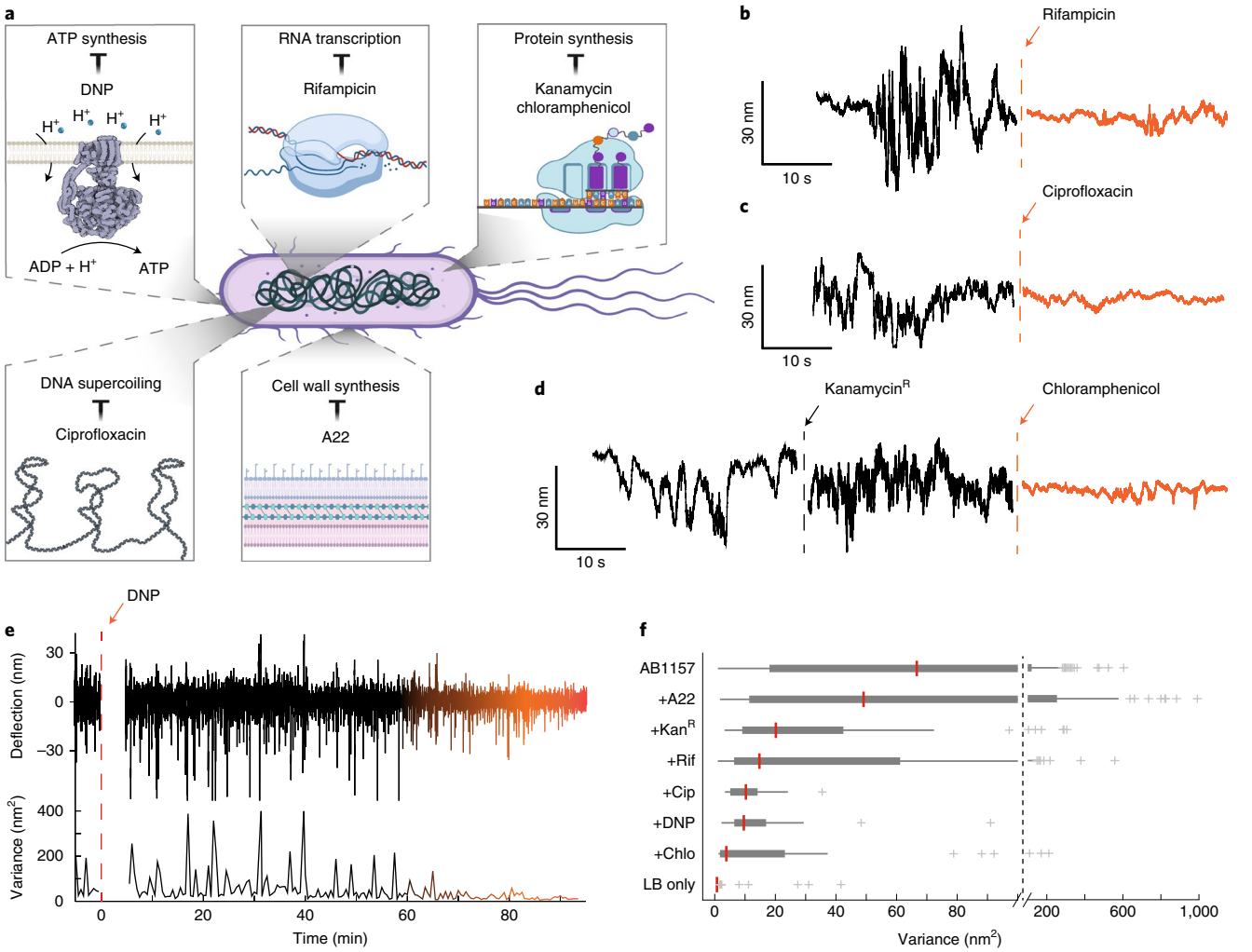

Fig. 4 | Single-cell antibiotic sensitivity screening using graphene. a, Schematic of antibiotics used in this work and their respective mode of action. **b**,**c**, Recorded motion of a drum with *E. coli* before (black) and after exposure to antibiotics (orange): rifampicin (**b**) and ciprofloxacin (**c**). **d**, Recorded motion of a drum with a kanamycin-resistant *E. coli* bacterium before (black), after 1 hour of exposure to kanamycin and subsequently after 1 h of exposure to chloramphenicol. **e**, Recorded deflection (upper trace) that starts 6 min after DNP drug injection at $t = 0$ min (vertical orange dashed line). A moving average is used to calculate the variance (below) using a window of 30 min. **f**, Box plot for all measurements after administering the corresponding drug to the *E. coli* strain AB1157 ($n = 277$), +A22 ($n = 108$), +kanamycin ($n = 33$), +rifampicin ($n = 83$), +ciprofloxacin ($n = 36$), +DNP ($n = 27$), +chloramphenicol ($n = 33$), as well as for empty control drums in LB ($n = 80$). Box plot indicates the 25th, 50th (red line is the median) and 75th percentiles, whereas whiskers extend to maximum 1.5 times the interquartile distance. Outliers are indicated with a cross.

Besides detecting differences in nanomotion between strains, or after administering antibiotics, the graphene platform also offers the possibility of real-time probing of the decrease in vibration amplitude, providing on-the-fly information on the route to bacterial death. From long-time trace measurements such as Fig. 4e (and Supplementary Note 6), we found that most of the nanomotion fades within the first hour after exposure to antibiotics. We also note that after adding the antibiotic the PSD drops down to the level of an empty drum (Supplementary Note 4). This experiment demonstrates the potential of graphene devices as an indicator of bacterial physiology, and opens new routes for determining the temporal response of bacteria to antibiotics at single-cell level.

Conclusions

We present an ultrasensitive platform that uses graphene drums to measure nanomotion of single bacterial cells. Single *E. coli* bacteria were observed to produce peak fluctuations of up to 60 nm in amplitude that corresponded to forces of up to 6 nN as inferred from the graphene membrane stiffness of $k \cong 0.1\,\mathrm{N\,m^{-1}}$ (Methods). These forces are larger than the typical forces generated by a single molecular motor[29] ($F \cong 10$ pN) or a single flagellar motor[30,31] ($F \cong 100$ pN), indicating that multiple molecular motors and flagella contribute collectively to the observed force. By comparing the nanomotion of different strains of bacteria, we conclude that flagellar motion is the main contributing factor to the nanoscale vibrations. It is worth noting, however, that flagellar motility is not the only source of nanomotion, as it was observed even in flagella-less *E. coli* and natural atrichous *B. subtillis* (Supplementary Fig. 5), albeit at significantly lower amplitude.

Our platform expands on the available tools for single-cell analysis, such as high-resolution fluorescence microscopy, and sets a new benchmark for sensitivity with respect to the available nanomotion method using cantilevers. Single-cell data have many useful properties; they allow for the identification and study of persister cells, which are related to the emergence of antibiotic resistance[32] within a population and can be obtained at a lower specimen concentration. In contrast to fluorescence microscopy, nanomotion detection

Table 1 | Efficacy of antibiotics measured 1 h after exposure

Antibiotic	Number of drums measured (*n*)	Median variance before exposure (nm^2)	Median variance 1 hour after exposure (nm^2)	*P* value
A22	108	66.7	49.1	0.83^{NS}
Kanamycin^R	33	32.3	20.2	0.11^{NS}
Rifampicin	83	92.6	14.7	≤0.0001****
Ciprofloxacin	36	18.8	10.3	0.00030***
DNP	27	94.8	9.6	≤0.0001****
Chloramphenicol	33	32.3	3.4	0.0091**

Median value of the variance before and after exposure are compared, and the probability (*P* value) that the drug has no effect on the nanomotion variance is evaluated using a two-tailed rank test. For all antibiotics except A22, a two-tailed Wilcoxon signed rank test is performed for paired measurements before and after exposure to the antibiotic. For A22, a two-tailed Wilcoxon rank sum test is performed with respect to *E. coli* AB1157. Superscript R indicates antibiotic resistance and significance is expressed using the asterisk convention.

is a label-free technique and thus can be applied directly on clinical samples for antibiotic sensitivity screening. Whereas cantilevers can be used to resolve nanomotion in a large aggregate of at least several hundreds of bacteria[4], a graphene drum accommodates single bacteria and its different geometry results in a reduced damping and thermal noise, allowing smaller forces to still be distinguished from the noise floor. Graphene is strong, inert, thin and couples well to light, which makes it stand out among two-dimensional materials as a support material for nanomotion sensing and is well-suited to be massively parallelized.

Recent reports call for the development of effective diagnostic tools to detect antimicrobial resistance and slow down the emergence of multi-drug resistant bacteria by prescribing the correct drug[33]. Our antibiotic susceptibility experiments demonstrated that the graphene drum sensing platform can trace the effect of antibiotics on bacterial nanomotion in real-time. This opens the way to fast, label-free susceptibility testing down to the single bacterial level (Supplementary Video). In comparison to other techniques for detecting antibiotic susceptibility[34], the method presented here stands out in terms of sensitivity and speed, offering the capability to quantify the nanomotion at the level of individual bacteria within a timeframe of 30 s. The small size of the graphene drums enables high-throughput sensing, allowing, in principle, millions of cells to be monitored in parallel in the presence of antibiotics. Similar benefits might apply in the field of personalized medicine, where the right antibiotic can be rapidly selected on the basis of the nanomotion response.

Furthermore, directed evolution experiments may benefit from this technique as a fast selection and screening method[35], as the density of over 10,000 nanomotion sensors per mm^2 can result in a greatly increased throughput as compared to 96-well plates or petri-dish culturing. With the significant reduction in size and increase in sensitivity presented in this work, nanomotion detection potentially can evolve into an important non-invasive monitoring tool in cell biology and provide new routes for rapid screening tests in personalized medicine and drug development.

Online content

Any methods, additional references, Nature Research reporting summaries, source data, extended data, supplementary information, acknowledgements, peer review information; details of author contributions and competing interests; and statements of data and code availability are available at https://doi.org/10.1038/s41565-022-01111-6.

Received: 3 November 2021; Accepted: 2 March 2022;
Published online: 18 April 2022

References

1. Glass, L. & Mackey, M. C. *From Clocks to Chaos: The Rhythms of Life* Vol. XVII (Princeton Univ. Press, 1988).
2. Longo, G. et al. Rapid detection of bacterial resistance to antibiotics using AFM cantilevers as nanomechanical sensors. *Nat. Nanotechnol.* **8**, 522–526 (2013).
3. Kohler, A. C., Venturelli, L., Longo, G., Dietler, G. & Kasas, S. Nanomotion detection based on atomic force microscopy cantilevers. *Cell Surf.* **5**, 100021 (2019).
4. Venturelli, L. et al. A perspective view on the nanomotion detection of living organisms and its features. *J. Mol. Recognit.* **33**, e2849 (2020).
5. Jülicher, F. Mechanical oscillations at the cellular scale. *C. R. Acad. Sci. IV* **2**, 849–860 (2001).
6. Ruggeri, F. S. et al. Amyloid single-cell cytotoxicity assays by nanomotion detection. *Cell Death Discov.* **3**, 17053 (2017).
7. Willaert, R. G. et al. Single yeast cell nanomotions correlate with cellular activity. *Sci. Adv.* **6**, eaba3139 (2020).
8. Kohler, A.-C. et al. Yeast nanometric scale oscillations highlights fibronectin induced changes in *C. albicans*. *Fermentation* **6**, 28 (2020).
9. Cadart, C., Venkova, L., Recho, P., Lagomarsino, M. C. & Piel, M. The physics of cell-size regulation across timescales. *Nat. Phys.* **15**, 993–1004 (2019).
10. Li, M., Xi, N., Wang, Y. & Liu, L. Advances in atomic force microscopy for single-cell analysis. *Nano Res.* **12**, 703–718 (2019).
11. Martínez-Martín, D. et al. Inertial picobalance reveals fast mass fluctuations in mammalian cells. *Nature* **550**, 500–505 (2017).
12. Krieg, M. et al. Atomic force microscopy-based mechanobiology. *Nat. Rev. Phys.* **1**, 41–57 (2019).
13. Arbore, C., Perego, L., Sergides, M. & Capitanio, M. Probing force in living cells with optical tweezers: from single-molecule mechanics to cell mechanotransduction. *Biophys. Rev.* **11**, 765–782 (2019).
14. Otto, O. et al. Real-time deformability cytometry: on-the-fly cell mechanical phenotyping. *Nat. Methods* **12**, 199–202 (2015).
15. Bennett, I., Pyne, A. L. B. & McKendry, R. A. Cantilever sensors for rapid optical antimicrobial sensitivity testing. *ACS Sens.* **5**, 3133–3139 (2020).
16. Syal, K. et al. Antimicrobial susceptibility test with plasmonic imaging and tracking of single bacterial motions on nanometer scale. *ACS Nano* **10**, 845–852 (2016).
17. Steeneken, P. G., Dolleman, R. J., Davidovikj, D., Alijani, F. & van der Zant, H. S. Dynamics of 2D material membranes. *2D Mater.* **8**, 042001 (2021).
18. Rosłoń, I. E. et al. High-frequency gas effusion through nanopores in suspended graphene. *Nat. Commun.* **11**, 6025 (2020).
19. Davidovikj, D. et al. Visualizing the motion of graphene nanodrums. *Nano Lett.* **16**, 2768–2773 (2016).
20. Lissandrello, C. et al. Nanomechanical motion of *Escherichia coli* adhered to a surface. *Appl. Phys. Lett.* **105**, 113701 (2014).
21. Barker, C. S., Prüß, B. M. & Matsumura, P. Increased motility of *Escherichia coli* by insertion sequence element integration into the regulatory region of the flhD operon. *J. Bacteriol.* **186**, 7529–7537 (2004).
22. Leatham, M. P. et al. Mouse intestine selects nonmotile *flhDC* mutants of *Escherichia coli* MG1655 with increased colonizing ability and better utilization of carbon sources. *Infect. Immun.* **73**, 8039–8049 (2005).
23. Sowa, Y. et al. Direct observation of steps in rotation of the bacterial flagellar motor. *Nature* **437**, 916–919 (2005).
24. Bremer, E., Silhavy, T. J. & Weinstock, G. M. Transposable lambda placMu bacteriophages for creating lacZ operon fusions and kanamycin resistance insertions in *Escherichia coli*. *J. Bacteriol.* **162**, 1092–1099 (1985).
25. Karczmarek, A. et al. DNA and origin region segregation are not affected by the transition from rod to sphere after inhibition of *Escherichia coli* MreB by A22. *Mol. Microbiol.* **65**, 51–A63 (2007).
26. Japaridze, A., Gogou, C., Kerssemakers, J. W., Nguyen, H. M. & Dekker, C. Direct observation of independently moving replisomes in *Escherichia coli*. *Nat. Commun.* **11**, 3109 (2020).
27. Wu, F. et al. Direct imaging of the circular chromosome in a live bacterium. *Nat. Commun.* **10**, 2194 (2019).
28. Wang, X. & Sherratt, D. J. Independent segregation of the two arms of the *Escherichia coli* ori region requires neither RNA synthesis nor MreB dynamics. *J. Bacteriol.* **192**, 6143–6153 (2010).
29. Visscher, K., Schnitzer, M. J. & Block, S. M. Single kinesin molecules studied with a molecular force clamp. *Nature* **400**, 184–189 (1999).
30. Ryu, W. S., Berry, R. M. & Berg, H. C. Torque-generating units of the flagellar motor of *Escherichia coli* have a high duty ratio. *Nature* **403**, 444–447 (2000).
31. Mandadapu, K. K., Nirody, J. A., Berry, R. M. & Oster, G. Mechanics of torque generation in the bacterial flagellar motor. *Proc. Natl Acad. Sci. USA* **112**, E4381–E4389 (2015).

32. Barrett, T. C., Mok, W. W., Murawski, A. M. & Brynildsen, M. P. Enhanced antibiotic resistance development from fluoroquinolone persisters after a single exposure to antibiotic. *Nat. Commun.* **10**, 1–11 (2019).
33. *No Time to Wait: Securing the Future from Drug-Resistant Infections* (WHO, 2019).
34. Van Belkum, A. et al. Innovative and rapid antimicrobial susceptibility testing systems. *Nat. Rev. Microbiol.* **18**, 299–311 (2020).
35. Cobb, R. E., Chao, R. & Zhao, H. Directed evolution: past, present, and future. *AIChE J.* **59**, 1432–1440 (2013).

Methods

Bacterial strains. For antibiotics susceptibility experiments, FW2179, a derivative of *E. coli* AB1157 strain, described previously in ref. [27], was used. Hyper-motile (MG1655(+IS1)), minimally motile (MG1655(−S1)), non-motile (MG1655ΔmotAB) and flagella-less (MG1655ΔfliC) strains that were described previously in ref. [36], were a kind gift from B. Beaumont from TU Delft.

Sample preparation. For experiments with *E. coli* cells, we grew cells in LB media overnight at 30 °C to reach the late exponential phase. On the day of the experiment, the overnight culture was refreshed (1:100 volume) for 2.5 h on fresh LB medium at 30 °C to reach an optical density (OD_{600}) of 0.2–0.3. Then 1 ml of the refreshed culture was mixed with APTES (Sigma-Aldrich) to reach a final concentration of 0.1% APTES (volumetric). This acts as a binder between the bacteria and the chips[37]. A cuvette with a graphene-covered chip inside was then filled with the solution. The chamber was left for 15 minutes in a horizontal position to deposit the bacteria on the surface. Afterwards, the chamber was placed in an upright position to prevent additional bacteria from depositing and maintain an average coverage of a single bacterium per drum. An optical microscope (Keyence VHX-7000) was used to inspect the sample. The cuvette was then placed in the optical nanomotion detection setup (Fig. 1a). The setup was equipped with nano positioners (Attocube ECSx5050) that allow for automated scanning over an array of drums. The motion of the bacterium was transduced on the drum and recorded using a digital oscilloscope (Rohde & Schwarz RTB2004). For each drum, a trace was recorded for at least 30 min with a sampling rate of at least 500 Hz. The measurements were performed in an air-conditioned room with a temperature of 21 °C. After measuring the sample for 1 h and collecting approximately 60 time-traces of different drums, antibiotics were added to the solution at the concentration given in Table 2. The antibiotic was left to work for 1 h (unless otherwise stated), and afterwards a new round of measurements was performed on the same array of graphene drums.

Substrates. The substrates were $5\times5\,mm^2$ silicon chips with a 285-nm layer of silicon oxide, which were patterned with circular holes by a reactive ion etch where the silicon acts as a stop layer. Chemical vapour-deposited bilayer graphene was supplied, transferred and suspended over the circular holes by Graphenea with a dry transfer method. The quality of the graphene drums was inspected by scanning electron microscopy and optical microscopy. Suspended circular drums with a diameter of 8 μm were used for the experiments.

Antibiotics. The antibiotics used in this work are listed in Table 2.

Amplitude calibration. Here we describe how the drum deflection $z(t)$ was obtained from the reflected intensity variations $I(t)$ of the red laser that was reflected by the photodiode voltage $V_{pd}(t)$. We first define the reflection coefficient $R(t)=I(t)/I_0$, where I_0 is the incident light intensity and $I(t)$ is the reflected light intensity. The reflection coefficient $R(t)$ depends on the optical characteristics of the cavity formed between the graphene and the silicon and the position $z(t)$ of the graphene membrane. Subsequently, light passes through three media with the following refractive indices: LB media with $n_{LB}=1.34–0.0007i$, graphene with $n_{gr}=2.7–1.6i$, air with $n_{air}=1$ and finally the light was reflected from the silicon mirror $n_{si}=4.2–0.06i$, where i is the imaginary unit. Together, the semitransparent graphene layer and the reflective silicon form a Fabry–Pérot cavity. The reflected light is modulated by the graphene drum moving through the optical field, and the reflection coefficient $R=I/I_0$ can be described by the following equation[38]

$$R=\left[\frac{r_1+r_2e^{-i\delta_1}+r_3e^{-i\delta_2}+r_1r_2r_3e^{-i(\delta_1+\delta_2)}}{1+r_1r_2e^{-i\delta_2}+r_1r_3e^{-i(\delta_1+\delta_2)}+r_2r_3e^{-i\delta_2}}\right]^2,$$

where $r_1=\frac{n_{LB}-n_{gr}}{n_{LB}+n_{gr}}$, $r_2=\frac{n_{gr}-n_{air}}{n_{gr}+n_{air}}$ and $r_3=\frac{n_{air}-n_{si}}{n_{air}+n_{si}}$, and the exponent δ is the phase difference that the light of wavelength λ acquires while travelling through a medium of thickness t. In this case $\delta_1=\frac{2\pi n_{gr}t_{gr}}{\lambda}$ and $\delta_2=\frac{2\pi n_{air}t_{air}}{\lambda}$, with $t_{air}=g+z(t)$. The reflectivity of the cavity depends on the number of graphene layers and the cavity depth, as plotted in Extended Data Fig. 1a, where the reflectivity for bilayer graphene is indicated by a red line. The design cavity depth is 285 nm, however, the drums bulged down by typically 60 nm under pressure of the liquid as can be seen in the liquid AFM image (Supplementary Note 5). Therefore, we consider that the effective cavity depth was $g=225$ nm. Then, we normalized the reflectivity by dividing it over R at a cavity depth of 225 nm (R_0), to find the slope around that point, which equals $\varphi=d(R(t)/R_0)/dz=-0.0038\,nm^{-1}$, as indicated in Extended Data Fig. 1b.

Data were gathered by an oscilloscope measuring the voltage $V_{pd}(t)$ from the photodiode that is proportional to the reflected light intensity and is operated in its linear range. The gathered time trace was normalized by division over its average, $V_{norm}=V_{pd}(t)/\langle V_{pd}(t)\rangle$ and a linear fit was subtracted from the data to eliminate the effects of drift during the measurement. Using the calibration factor φ, the deflection $z(t)$ was calculated as $z(t)=[V_{pd}(t)/\langle V_{pd}(t)\rangle-1]/\varphi$.

While the current nanomotion detection technique works well for qualitative analysis of changes in the bacterial nanomotion in time, there are several approximations made in the conversion from the nanomotion-induced light-intensity variations detected by the photodiode to a nanomotion amplitude in nm. First of all, the nanomotion generated by a bacterium may depend on its position on the drum, which could cause experimental variations. In our calculations of the force, we assume that a single bacterium is centred on the drum. Moreover, in the optical model, the cavity underneath the graphene is assumed to be filled by air. The use of bilayer graphene minimizes the chances that small defects cause leakage and liquid AFM measurements (Supplementary Note 5) also showed that the graphene membranes bulge down, which is to be expected if the cavity is air filled. Finally, the bacterium is attached to the surface of the graphene and is likely to be in the laser beam path. The refractive index of an *E. coli* bacterium[39,40] ($n=1.33$) is very close to that of the LB medium ($n=1.34$), causing the bacteria to be nearly transparent, and therefore we estimate this to have a negligible impact on the nanomotion amplitude determination.

Table 2 | Table describing the types and concentrations of antibiotics used (Fig. 4a)

Antibiotic	Target	Mechanism	Concentration
A22	Cell-wall synthesis	Inhibits MreB filament polymerization	5 μg ml^{-1}
Kanamycin	Translation	Binds ribosome and interferes in elongation of polypeptide chain elongation	50 μg ml^{-1}
Chloramphenicol	Translation	Binds to ribosome and inhibits binding of transfer RNA	34 μg ml^{-1}
Ciprofloxacin	DNA supercoiling homeostasis	Traps topoisomerase and DNA in a complex, inhibits DNA rejoining after cleavage	15 μg ml^{-1}
Cadaverine	Ion transport	Induces closure of porins and inhibits ion transport over the membrane	50 mM
Rifampicin	Transcription	Binds to RNA polymerase and blocks the elongating RNA molecule	50 μg ml^{-1}
DNP	H^+ gradient across the membrane	Inhibits ATP synthesis	2 mM

Estimation of the stiffness and noise floor of a graphene drum. We estimate the stiffness k_1 of the circular graphene drum with area $A=50\,\mu m^2$ on the basis of the deflection z at the centre of the membrane with respect to a flat configuration induced by uniform liquid pressure P in the cuvette. Hooke's law prescribes that the stiffness can be found by equating forces:

$$kz=PA$$

The graphene drum is immersed 1 cm below the surface of the liquid and is therefore under a uniform pressure of 100 Pa. Under these conditions, the graphene is found to deflect 60 nm downwards, as measured by liquid AFM (Supplementary Note 5). By inserting these values in the equation above, we find $k=0.14\,N\,m^{-1}$. Our estimate of the stiffness of graphene drums corresponds to values reported in literature[41–43], which typically range from 0.05 to 1 N m^{-1}.

Next, we estimate the amplitude noise floor of the empty graphene drums to estimate the minimum detectable nanomotion level. The mean square force noise on a harmonic oscillator with a damping constant c is given by $F^2=4\,k_B\,Tc\,BW$, where k_B is Boltzmann's constant, T is the temperature and BW is the measurement bandwidth[17]. Far below the resonance frequency, the variance in the amplitude is given by $\sigma_{empty}=F^2/k^2$, which is proportional to c. For a circular graphene drum, the damping constant c (N s^{-1} m^{-1}) can be roughly approximated from Stokes' law, assuming a spherical particle moving through a fluid, $c=6\pi\mu R$, where for our drum the radius $R=4\,\mu m$ and $\mu=0.001$ Pa s for water at 20 °C, which yields $c=7.5\times10^{-8}\,N\,s\,m^{-1}$. In the case of cantilevers[44], typical damping

constants are $c \cong 1 \times 10^{-6}$ N s m^{-1}. Thus the empty drums have a damping constant and nanomotion variance that is over a factor of ten lower than that of AFM cantilevers, resulting in a higher signal-to-noise ratio, which facilitates single-cell motion detection.

Statistics. Since the data reported in the paper are not normally distributed, we relied on non-parametric tests for statistics. We represent the median and quartiles of data in boxplots, in accordance with the use of non-parametric tests. We use a signed rank test whenever repeated measurements on the same drum are available (that is, antibiotic susceptibility test), and rank sum test for comparison between strains. We used MATLAB's built-in functions for statistical analysis. All statistical tests were two-sided. On all figures, the following conventions are used: not significant (NS) $0.05 < P$, *$0.01 < P < 0.05$, **$0.001 < P < 0.01$, ***$0.0001 < P < 0.001$, ****$P < 0.0001$. We report a significant difference in results if $P < 0.01$.

Reporting Summary. Further information on research design is available in the Nature Research Reporting Summary linked to this article.

Data availability

The raw datasets of this study are available from the corresponding author on request.

References

36. Gauger, E. J. et al. Role of motility and the *flhDC* operon in *Escherichia coli* MG1655 colonization of the mouse intestine. *Infect. Immun.* **75**, 3315–3324 (2007).
37. Louise Meyer, R. et al. Immobilisation of living bacteria for AFM imaging under physiological conditions. *Ultramicroscopy* **110**, 1349–1357 (2010).
38. Blake, P. et al. Making graphene visible. *Appl. Phys. Lett.* **91**, 063124 (2007).
39. Balaev, A., Dvoretski, K. & Doubrovski, V. *Refractive Index of Escherichia coli Cells* 4707 SFM (SPIE, 2002).
40. Liu, P. Y. et al. Real-time measurement of single bacterium's refractive index using optofluidic immersion refractometry. *Procedia Eng.* **87**, 356–359 (2014).
41. Suk, J. W., Piner, R. D., An, J. & Ruoff, R. S. Mechanical properties of monolayer graphene oxide. *ACS Nano* **4**, 6557–6564 (2010).
42. Davidovikj, D. et al. Nonlinear dynamic characterization of two-dimensional materials. *Nat. Commun.* **8**, 2153 (2017).
43. Castellanos-Gomez, A., Singh, V., van der Zant, H. S. & Steele, G. A. Mechanics of freely-suspended ultrathin layered materials. *Ann. Phys.* **527**, 27–44 (2015).
44. Maali, A. et al. in *Applied Scanning Probe Methods XII: Characterization* (eds Bhushan, B. & Fuchs, H.) 149–164 (Springer, 2009).

Acknowledgements

Financial support was provided from the European Union's Horizon 2020 research and innovation programme under ERC starting grant ENIGMA (no. 802093, F.A. and I.E.R.), ERC PoC GRAPHFITI (no. 966720, F.A. and A.J.), Graphene Flagship (grant nos. 785219 and 881603, P.S.) and the ERC Advanced Grant LoopingDNA (no. 883684, C.D.), as well as the Netherlands Organization for Scientific Research (NWO/OCW), as part of the NanoFront and BaSyC programmes and by the Swiss National Science Foundation (grant no. P300P2_177768, A.J.). We acknowledge Graphenea for providing and transferring the bilayer graphene used in this research. We thank M. Tišma for help in the wetlab, B. Beaumont and A. Derumigny for discussions, and T. de Visser, S. Mohammad, N. Wansink and S. van Putten for their contributions to the nanomotion detection setup. Schematics in Figs. 3a and 4a were created with Biorender.com.

Author contributions

A.J. and F.A. conceived the idea. I.E.R. and A.J. collected the data. I.E.R. constructed the setup and performed the interferometry experiments. A.J. performed the bacterial manipulation. All authors designed the experiments. The project was supervised by C.D., P.G.S. and F.A. All authors contributed to the data analysis, interpretation of the results and writing of the manuscript.

Competing interests

The authors have a patent on the techniques described in the paper (patent no. WO/2021/112666).

Additional information

Extended data are available for this paper at https://doi.org/10.1038/s41565-022-01111-6.

Supplementary information The online version contains supplementary material available at https://doi.org/10.1038/s41565-022-01111-6.

Correspondence and requests for materials should be addressed to Farbod Alijani.

Peer review information *Nature Nanotechnology* thanks the anonymous reviewers for their contribution to the peer review of this work.

Reprints and permissions information is available at www.nature.com/reprints.

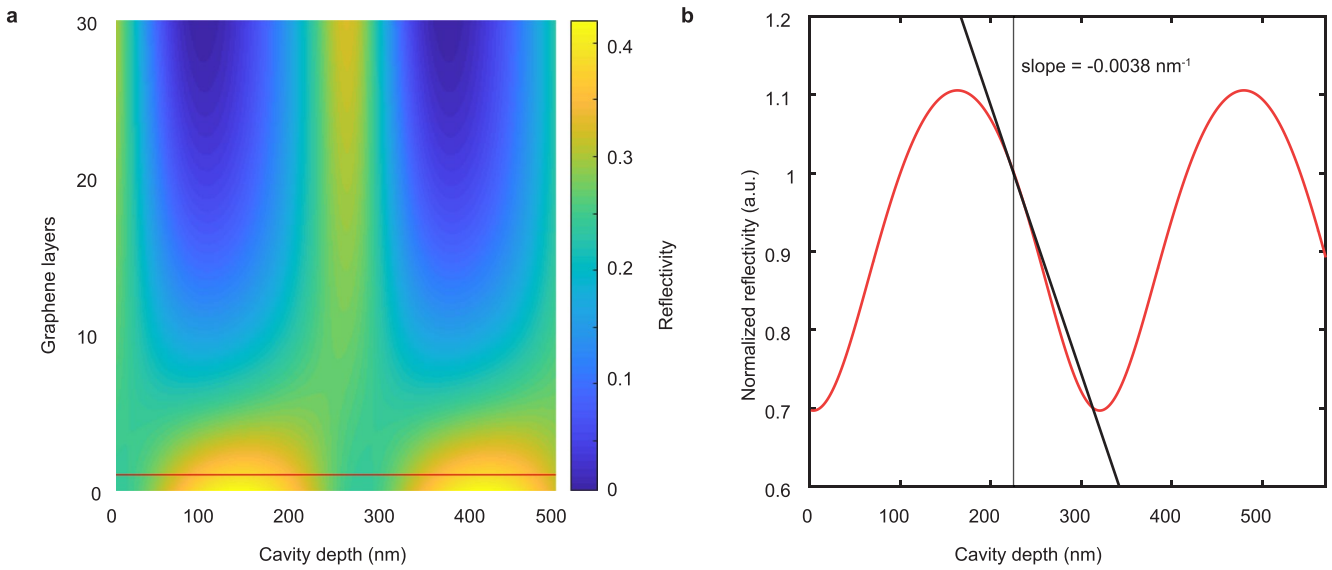

Extended Data Fig. 1 | Reflectivity of the Fabry-Pérot cavity formed by suspended graphene. a, Reflectivity as a function of number of graphene layers and cavity depth. Values for bilayer graphene are indicated by a red line. **b**, The reflectivity change is normalized with respect to the natural position of the graphene drum. By determining the slope around this point, a sensitivity $\varphi = -0.0038\,\mathrm{nm}^{-1}$ is found.

nature portfolio

Corresponding author(s): F.Alijani

Last updated by author(s): Feb 10, 2022

Reporting Summary

Nature Portfolio wishes to improve the reproducibility of the work that we publish. This form provides structure for consistency and transparency in reporting. For further information on Nature Portfolio policies, see our Editorial Policies and the Editorial Policy Checklist.

Statistics

For all statistical analyses, confirm that the following items are present in the figure legend, table legend, main text, or Methods section.

n/a	Confirmed	
☐	☒	The exact sample size (*n*) for each experimental group/condition, given as a discrete number and unit of measurement
☐	☒	A statement on whether measurements were taken from distinct samples or whether the same sample was measured repeatedly
☐	☒	The statistical test(s) used AND whether they are one- or two-sided *Only common tests should be described solely by name; describe more complex techniques in the Methods section.*
☒	☐	A description of all covariates tested
☒	☐	A description of any assumptions or corrections, such as tests of normality and adjustment for multiple comparisons
☐	☒	A full description of the statistical parameters including central tendency (e.g. means) or other basic estimates (e.g. regression coefficient) AND variation (e.g. standard deviation) or associated estimates of uncertainty (e.g. confidence intervals)
☐	☒	For null hypothesis testing, the test statistic (e.g. *F*, *t*, *r*) with confidence intervals, effect sizes, degrees of freedom and *P* value noted *Give P values as exact values whenever suitable.*
☒	☐	For Bayesian analysis, information on the choice of priors and Markov chain Monte Carlo settings
☒	☐	For hierarchical and complex designs, identification of the appropriate level for tests and full reporting of outcomes
☒	☐	Estimates of effect sizes (e.g. Cohen's *d*, Pearson's *r*), indicating how they were calculated

Our web collection on statistics for biologists contains articles on many of the points above.

Software and code

Policy information about availability of computer code

Data collection	Build-in Matlab R2018b functions were used for data collection.
Data analysis	Build-in Matlab R2018b functions were used for data analysis.

For manuscripts utilizing custom algorithms or software that are central to the research but not yet described in published literature, software must be made available to editors and reviewers. We strongly encourage code deposition in a community repository (e.g. GitHub). See the Nature Portfolio guidelines for submitting code & software for further information.

Data

Policy information about availability of data

All manuscripts must include a data availability statement. This statement should provide the following information, where applicable:

- Accession codes, unique identifiers, or web links for publicly available datasets
- A description of any restrictions on data availability
- For clinical datasets or third party data, please ensure that the statement adheres to our policy

The raw datasets of this study are available from the corresponding author on request.

Field-specific reporting

Please select the one below that is the best fit for your research. If you are not sure, read the appropriate sections before making your selection.

☒ Life sciences ☐ Behavioural & social sciences ☐ Ecological, evolutionary & environmental sciences

For a reference copy of the document with all sections, see nature.com/documents/nr-reporting-summary-flat.pdf

Life sciences study design

All studies must disclose on these points even when the disclosure is negative.

Sample size	Sample sizes are determined by the number of intact drums available for measurement within a reasonable time window (e.g. 1 hour, n = 20 to 200).
Data exclusions	Experiments in which cells were lysed or formed aggregates (based on optical images) were excluded from the analysis.
Replication	Experiments were replicated with various antibiotics and strains as described in the manuscript.
Randomization	Experiments were performed on E.coli cells from the same strain.
Blinding	Blinding was not relevant to the study.

Reporting for specific materials, systems and methods

We require information from authors about some types of materials, experimental systems and methods used in many studies. Here, indicate whether each material, system or method listed is relevant to your study. If you are not sure if a list item applies to your research, read the appropriate section before selecting a response.

Materials & experimental systems

n/a	Involved in the study
☒	☐ Antibodies
☒	☐ Eukaryotic cell lines
☒	☐ Palaeontology and archaeology
☒	☐ Animals and other organisms
☒	☐ Human research participants
☒	☐ Clinical data
☒	☐ Dual use research of concern

Methods

n/a	Involved in the study
☒	☐ ChIP-seq
☒	☐ Flow cytometry
☒	☐ MRI-based neuroimaging